PHYSICAL REVIEW D

PARTICLES AND FIELDS

THIRD SERIES, VOLUME 40, NUMBER 7 1 OCTOBER 1989

Experimental study of muon bundles observed in the Fréjus detector

Ch. Berger, M. Fröhlich, H. Mönch, R. Nisius, F. Raupach, and P. Schleper
I. Physikalisches Institut der Rheinisch-Westfälische Technische Hochschule Aachen, D-5100 Aachen, Federal Republic of Germany

Y. Benadjal, D. Blum, C. Bourdarios, B. Dudelzak, P. Eschstruth, S. Jullian, D. Lalanne, F. Laplanche, C. Longuemare, C. Paulot, O. Perdereau, Ph. Roy, and G. Szklarz
Laboratoire de l'Accélérateur Linéaire, Centre d'Orsay, Bâtiment 200, F-91405 Orsay, France

L. Behr, B. Degrange, Y. Minet, U. Nguyen-Khac, P. Serri, S. Tisserant, and R. D. Tripp*
Laboratoire de Physique Nucléaire des Hautes Énergies, Ecole Polytechnique, Route de Saclay, F-91128 Palaiseau, France

C. Arpesella,† P. Bareyre, R. Barloutaud, A. Borg, G. Chardin, J. Ernwein, J. F. Glicenstein, L. Mosca, and L. Moscoso
Département de Physique des Particules Élémentaires, Saclay, Boîte Postale No. 2, F-91191 Gif-sur-Yvette, France

J. Becker, K. H. Becker, H. J. Daum, S. Demski, B. Jacobi, B. Kuznik, R. Mayer,‡ H. Meyer, R. Möller, M. Schubnell, B. Seyffert, Y. Wei, and P. Wintgen§
Universität-Gesamthochschule Wuppertal, D-5600 Wuppertal 1, Federal Republic of Germany
(Fréjus Collaboration)
(Received 5 May 1989)

The present study is based on a sample of 407 775 single muons and 12 559 muon bundles with zenith angles smaller than 60°, observed in the 12.3 m×6 m×6 m Fréjus proton-decay detector, at a depth of 4850 hg/cm^2. The variation of the vertical muon intensity with depth is given. Using a maximum-likelihood method, the muon lateral distribution of underground bundles is investigated as a function of muon multiplicity and zenith angle. The same method yields the true multiplicity distribution at the site depth, corrected for all detection effects.

I. INTRODUCTION

The study of muon bundles observed in deep-underground experiments provides some clues on primary-cosmic-ray composition in the PeV range.[1,2] In this energy region, the cosmic-ray flux is too low to allow for direct measurements and the data of surface arrays or of underground detectors must be interpreted by means of a complex simulation starting from the primary spectrum and composition, following the development of the extensive air showers and finally reproducing all the experimental effects. Moreover, models proposing very different primary compositions in the PeV range are in competition[3] since they are only constrained by the all-particle spectrum and the composition measured below 10 TeV.

As far as underground experiments are concerned, most of the former detectors were small compared to typical sizes of underground showers[2] and the interpretation of the data consequently relied on the lateral distribution assumed in the simulation. The Fréjus proton-decay detector provides an average detection area of 100 m^2, whereas the typical distance between a muon and the shower axis is 3.3 m; its very fine grain (0.5 cm) allows a clear separation of close-packed muons. It is then possible to use the observed lateral distribution to correct for detector-size effects (as well as for other experimental biases) and to obtain the true muon multiplicity distribution at the site depth. Moreover, because of the large available statistics, the variations of the lateral distribution with both multiplicity and zenith angle are investigated and taken into account. These corrected data provide more constraining tests of air-shower simulations from both points of view of primary composition and of

hadronic interactions in the 100–1000-TeV range. This paper is devoted to the presentation of the experimental data; the interpretation in terms of primary-cosmic-ray composition will be given in a separate publication.

II. SITE AND EXPERIMENT

The underground laboratory is located at the center of the Fréjus highway tunnel connecting Modane (France) to Bardonecchia (Italy) under the Alps. The average rock cover amounts to 1780 m (4850 hg/cm^2). The geological structure is quite homogeneous in a large area,[4] as has been confirmed from various rock samples taken both in the tunnel and at the ground level. The characteristics of the Fréjus rock and the detailed topographical structure (which are relevant for the simulation of underground showers to be compared with the results presented here) are found in the Appendix. In the following, slant depths will be converted into hg/cm^2 of standard rock according to the data of the Appendix. The data presented in this paper are restricted to zenith angles smaller than 60°; this ensures a good knowledge of the topography of the mountain, which is necessary for further interpretation of the data.

The Fréjus nucleon-decay detector has been described in detail in Ref. 5. It is a parallelepiped (12.3 m long, with a 6×6 m cross section) consisting of 912 vertical planes of flash chambers interspersed with 113 planes of Geiger tubes. Detection planes alternately consist of horizontal and vertical tubes providing two orthogonal views. The 40 000 Geiger counters are used to trigger the flash chambers (934 000 cells with 5×5 mm cross section). The experiment started in February 1984, while part of the detection modules were being mounted. The detector reached its final size in June 1985. The data presented here were taken from December 1984 (80% of the final detector being active) to the end of the experiment in September 1988, corresponding to 24 600 hours of live time, most of them with the complete detector.

III. THE EVENT SAMPLES

Events were scanned and tagged by physicists at run time. This classification was further checked off line by a pattern recognition program, reconstructing single muons with an efficiency of 92%. Events with at least two muons (referred to as multimuon events in the following) are selected by the tagging procedure with less than 0.2% loss. Two kinds of selections were carried out, corresponding to the two following studies.

A. Muon vertical intensity as a function of depth

In order to determine the vertical intensity of muons I_0 as a function of depth h, it is necessary to restrict to those muons with a small angular error, allowing a good determination of the slant depth. Therefore, the following cuts were applied. Events with a muon almost parallel to the detection planes (angle with the planes smaller than 7°) were rejected. Furthermore, a muon path length greater than 1 m within the detector was required. These cuts ensure a high trigger and reconstruction efficiency (>99.5%) as well as a good accuracy on the muon direction. The slant depth of rock crossed by the muon was determined from the map given in the Appendix. The intensity of muons at zenith angle θ was assumed to be related to the vertical intensity I_0 through the classic relation $I(h,\theta)=I_0(h)/\cos\theta$, valid for muons of atmospheric origin in the relevant range of zenith angle ($\theta<60°$). Therefore, the vertical intensity in a given depth interval ($h\pm\Delta h/2$) was obtained from events with corresponding slant depths, by giving them the following weights:

$$w_i=\frac{m_i\cos\theta_i}{S_i\epsilon_i\Delta\Omega_h\Delta t}$$

in which m_i is the observed muon multiplicity in event i, S_i is the detector projected area as seen from the shower direction and corrected for the path length requirement explained above, ϵ_i is the trigger and reconstruction efficiency, $\Delta\Omega_h$ is the solid angle corresponding to the slant depth interval, corrected for effects of the angular cut, Δt is the live time of the experiment. A further correction was applied in order to take account of the nonuniformity of the h distribution in a given depth interval.

The relation $I_0(h)$ obtained from a sample of 317 556 single muon events and 10 390 multimuon events is shown in Fig. 1. For h lower than 10^4 hg/cm^2, this relation is well fitted by the formula

$$I_0(h)=K_0\left[\frac{h_0}{h}\right]^2\exp(-h/h_0)$$

with

$$K_0=(1.96\pm0.09)\times10^{-2}\ \mathrm{m^{-2}s^{-1}sr^{-1}}\ ,$$

$$h_0=1184\pm8(\mathrm{stat})\pm6(\mathrm{syst})\ \mathrm{hg/cm^2}\ ,$$

the correlation coefficient being −0.995.

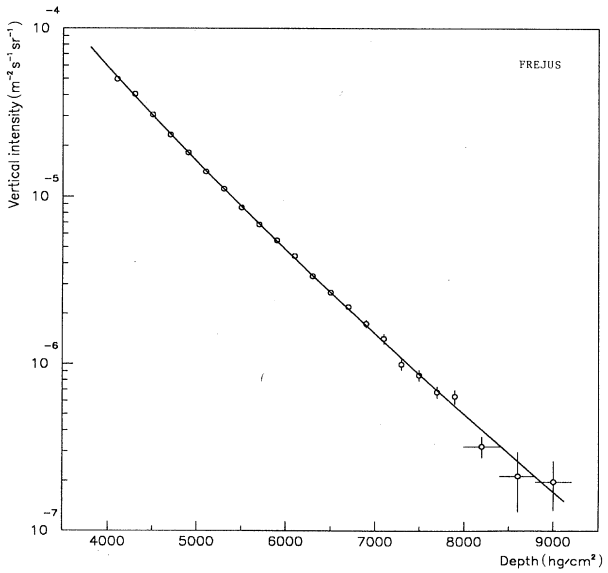

FIG. 1. Muon vertical intensity vs depth. Systematic errors in the determination of h (see text) are not shown in this figure.

The systematic error accounts for uncertainties in average rock density and composition, affecting the conversion of h into hg/cm^2 of standard rock. The error on $I_0(h)$ is dominated by the systematics for the range of depths covered in this experiment. In particular, for $h_1 = 5000$ hg/cm^2,

$$I_0(h_1) = [1.61 \pm 0.01(\text{stat}) \pm 0.05(\text{syst})] 10^{-5} \text{ m}^{-2}\text{s}^{-1}\text{sr}^{-1}$$

and, for $h_2 = 7500$ hg/cm^2,

$$I_0(h_2) = [8.66 \pm 0.13(\text{stat}) \pm 0.36(\text{syst})] 10^{-7} \text{m}^{-2}\text{s}^{-1}\text{sr}^{-1} .$$

These results are in good agreement with the data of previous experiments.[6]

B. Muon bundles

The study of multimuon events (see example in Fig. 2) was carried out by using a less restrictive selection. For each event, the result of the spatial reconstruction of the muons was visually checked by a physicist using an interactive graphic terminal, allowing to perform a new reconstruction with the help of the operator in case of failure of the automatic procedure (e.g., track-matching failure). As in the preceding study, events with a muon at small angle with respect to the detection planes were rejected, but here a less restrictive cut of 3° was applied. The overall event loss due to trigger inefficiency and to the preceding cut amounts to 10.6% and is found to be independent of the multiplicity within the errors. In the selected sample, the event multiplicity does not take account of those muons stopping within the detector or showing visible multiple scattering ($\sim 1\%$ of muons). With this restriction, the average opening angle of a muon pair is 1.1° (with 1.7° rms deviation). In a given event, the direction of the bundle was determined by averaging the direction vectors of all muons, each one being given a weight proportional to its total path length within the detector. The distance between two muons was defined by using the intersection points of their tracks with the plane passing by the center of the detector and orthogonal to the incident direction. The zenith angle of the bundle was further required to be less than 60° as indicated above. Fluxes will be given within the corresponding solid angle. It should be noted that the number of multimuon events at larger zenith angles is only 10% of the whole statistics.

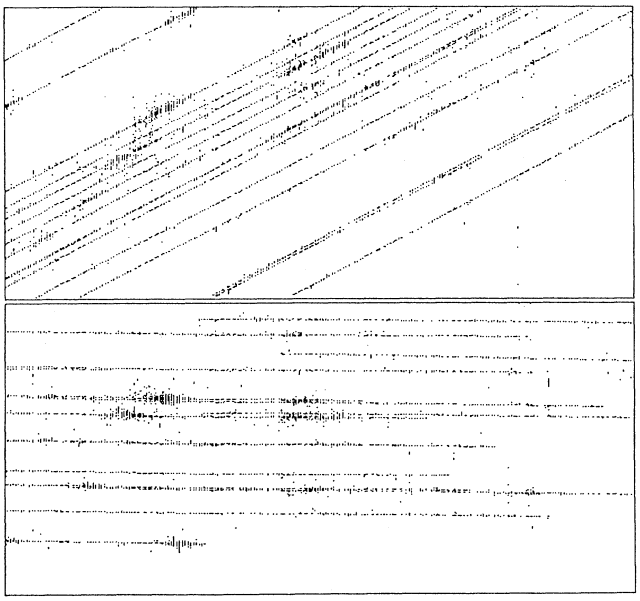

FIG. 2. A muon bundle observed in the Fréjus detector (12.3 m×6 m ×6 m).

The preceding selection yields a sample of 12 559 muon bundles. The statistics for each observed multiplicity are given in Table I and displayed in Fig. 3.

IV. CORRECTION OF DETECTION EFFECTS

A. The correction method

Because of the limited size of the detector, only a part of the underground shower is generally observed. However, the dimensions of the detector are large compared to the typical distance between a muon and the shower axis at the level of the laboratory (~ 3.3 m). Consequently, the multiplicity distribution at the site depth can be well determined by means of a maximum-likelihood method because the full information of each event can be used: namely, the number m of detected muons, the zenith and azimuth angles θ and ϕ of the incident direction, the position of each track within the apparatus, defined by 2-dimensional vectors $\vec{r}_k$ ($k = 1, \ldots, m$) orthogonal to the shower direction. This set of measured quantities is referred to as $\{x\}$ in the following.

In the correction method, the shape of the lateral dis-

TABLE I. Observed muon multiplicity distribution.

Observed multiplicity m	Number of events
2	10 379
3	1 490
4	401
5	118
6	63
7	33
8	16
9	11
10	12
11	6
12	3
13	6
14	3
15	7
16	3
17	3
18	2
19	1
20	1
21	0
22	0
23	0
24	0
25	1

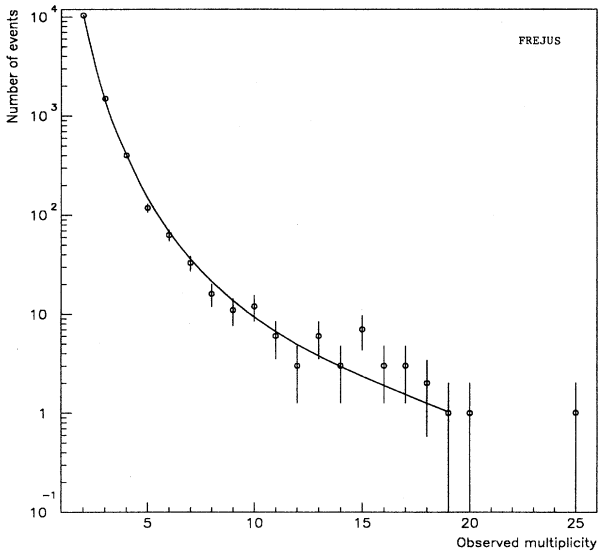

FIG. 3. Observed muon multiplicity distribution. The curve represents the distribution expected from formula (7) using the fitted values of ν_1 and a quoted in the text and taking account of detection biases. The curve is shown for observed multiplicities m lower than 20, for which the contribution of events with true multiplicities n greater than 30 is actually negligible. For practical reasons, the true multiplicity was limited to $n=30$ in the calculation.

tribution is assumed to be[7]

$$\frac{dN}{dr}=\frac{r}{r_0^2}e^{-r/r_0} \tag{1}$$

in which r is the distance between the muon and the unknown shower axis and r_0: a characteristic distance to be fitted from the data.[8] This last quantity is further allowed to vary both with the muon multiplicity and with the incident direction. Actually, the values of r_0 fitted from the maximum-likelihood method using formula (1) are found to reproduce the distribution of the distances between observed muon tracks, as shown in Fig. 4. This

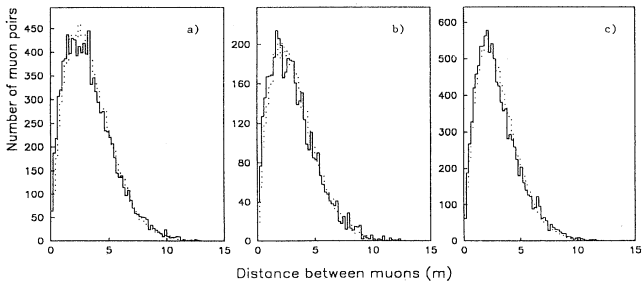

FIG. 4. Distributions of the distances between observed muon tracks (solid line). (a) Events with two observed muons. (b) Events with three observed muons. (c) Events with at least four observed muons. The dotted histograms represent the distributions expected from the lateral distribution and from the multiplicity distribution fitted by the maximum-likelihood method explained in the text, when detection effects are taken into account.

provides a consistency check of the method and of the parametrization chosen in formula (1).

Let μ_n be the expectation value of the number of events with n muons at the site depth in the present exposure and $P_n(\{x\}_i)$ the probability density functions for observing the set $\{x\}_i$ of measured quantities in event i, (n is thus the true multiplicity, to be distinguished from the observed multiplicity $m \le n$). The probability density function for obtaining the observed event sample is[9]

$$\mathcal{L}=\frac{1}{N!}\exp\left[-\sum_n \mu_n\right]\prod_{i=1}^{N}\left[\sum_n \mu_n P_n(\{x_i\})\right] \tag{2}$$

(N is the total number of collected events). The expectation values μ_n and the probability densities $P_n(\{x_i\})$ can be expressed as functions of the intensities $I_n(\theta,\phi)$ for various multiplicities and of the relevant characteristic distances. The quantity $\mathcal{L}$ given by formula (2) is thus considered as a likelihood function and maximized with respect to these parameters. Single-muon events are not included in the present likelihood calculation, in order to avoid prohibitive computing time. A further assumption used in the determination of $\mathcal{L}$ is that the angular distribution of the bundle direction is independent of the multiplicity. As a matter of fact, we have checked on raw data that the angular distributions of events with different observed multiplicities ($m=2$, $m=3$, $m\ge 4$) were compatible. Furthermore, the sample was divided into eight parts corresponding to different intervals in zenith angle, which were analyzed independently. Thus, the preceding approximation is certainly reasonable within a limited range in zenith angle; it will be further checked (Fig. 7) that the corrected flux ratios found in each of these eight intervals are compatible with each other. With this assumption, the intensity of muon bundles with n muons $I_n(\theta,\phi)$ can be factorized as $I_n(\theta,\phi)=[f(\theta,\phi)/\Delta\Omega]\Phi_n$, where Φ_n is the average muon flux, and $f(\theta,\phi)$ accounts for the angular distribution in the solid angle $\Delta\Omega=\pi$ steradians defined by the restriction $\theta<60°$, with the normalization $\int_{\Delta\Omega} f(\theta,\phi)d\Omega=1$.

The probability density $P_n(\{x\})$ for a given event ($\{x\}=\{m,\theta,\phi,\bar{r}_1,\ldots,\bar{r}_m\}$) can be written in the form

$$P_n(\{x\})=\frac{1}{A_n}f(\theta,\phi)\int\begin{bmatrix}n\\m\end{bmatrix}\left[\prod_{k=1}^{m}p_{r_0}(\bar{\xi},\bar{r}_j)\right]\times[1-S_{r_0}(\bar{\xi})]^{n-m}d_2\xi \tag{3}$$

in which $p_{r_0}(\bar{\xi},\bar{r}_k)$ is the probability density for finding a muon at position $\bar{r}_k$ when the shower axis is at position $\bar{\xi}$, and $S_{r_0}(\bar{\xi})=\int_{\text{detector}}p_{r_0}(\bar{\xi},\bar{r})d_2r$ is the probability that a muon from the same shower hit the detector; the surface integral in (3) is taken over the whole plane orthogonal to the bundle direction. The normalization factor A_n must satisfy $\int P_n\{x\}d\{x\}=1$: i.e.,

$$\sum_{2\le m\le n}\int P_n(\theta,\phi,\bar{r}_1,\ldots,\bar{r}_m)d\Omega\, d_2r_1\cdots d_2r_m=1\ .$$

Thus A_n is given by the formula

$$A_n = \sum_{2 \le m \le n} \int f(\theta,\phi) \begin{bmatrix} n \\ m \end{bmatrix} \times S_{r_0}^m(\bar{\xi})[1-S_{r_0}(\bar{\xi})]^{n-m} d\Omega\, d_2\xi \ . \quad (4)$$

This quantity, which has the dimension of an area (as $d_2\xi$), naturally relates the expected number of events with n muons at the site depth, μ_n, to the corresponding flux Φ_n:

$$\mu_n = A_n \Phi_n \Delta t \ , \quad (5)$$

Δt being the live time of the experiment.

The area A_n measures the capability of the detector to observe at least two muons in a bundle with multiplicity n; (Fig. 5). Substituting the expressions (3), (4), and (5) into (2), one finds the likelihood $\mathcal{L}$ as a function of the fluxes Φ_n and of the relevant characteristic distances.

B. Results on the lateral distribution

The distance r_0 characterizing the lateral distribution was investigated as a function of muon multiplicity, zenith angle, azimuth angle, and slant depth in the range 4400–5300 hg/cm^2 corresponding to 70% of the data. Only the first two parameters were found to influence r_0 significantly.

1. Dependence on muon multiplicity

In a first step, the maximum-likelihood method was used, assuming a single value of r_0 in a sample restricted to a minimal observed multiplicity m_0. A significant decrease in r_0 was observed when m_0 varied from 2 to 4; above this multiplicity all fitted values of r_0 were found to be compatible with each other.

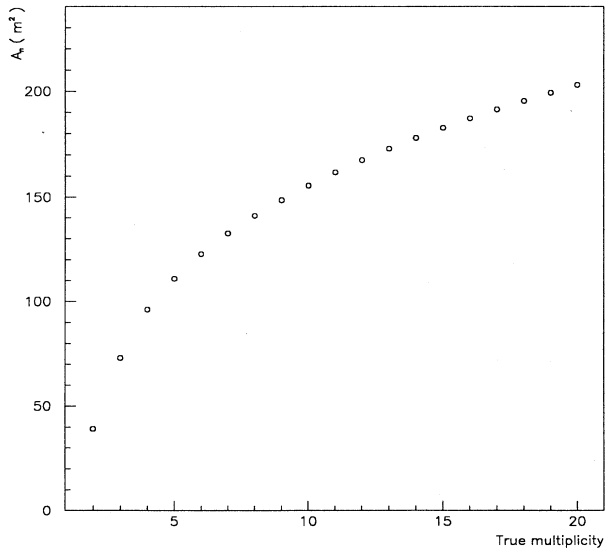

FIG. 5. A_n as a function of true muon multiplicity n. A_n is an area measuring the capability of the detector to observe at least two muons in a bundle with multiplicity n (see text).

A second maximum-likelihood fit was then performed assuming three different values of r_0, corresponding to true multiplicities $n=2$, $n=3$, and $n \ge 4$. Results, given in Table II(a), show a very significant difference between samples with $n=2$ and $n \ge 4$, respectively.

2. Dependence on zenith angle

The total sample was then divided into eight parts with similar statistics corresponding to different intervals in the zenith angle θ. In each subsample, r_0 was assumed to be different for $n \le 3$ and $n \ge 4$. The results of the maximum-likelihood fit are given in Table II(b) and displayed in Fig. 6. A linear dependence of r_0 with $\cos\theta$ can be fitted:

$$r_0(\cos\theta) = r_0(\gamma_n) + \alpha_n(\cos\theta - \gamma_n) \quad (6)$$

in which γ_n is chosen in such a way that α_n and $r_0(\gamma_n)$ be decorrelated (γ_n is the average value of $\cos\theta$ in the relevant sample). Results are given in Table II(c). If a single slope parameter α is chosen, one finds

$$\alpha = -77.5 \pm 12.0 \text{ cm}$$

and the difference $\Delta r_0 = r_0(n \le 3) - r_0(n \ge 4)$ is found to be 32 ± 3 cm.

In the following analysis, r_0 is assumed to vary both with multiplicity and $\cos\theta$; three values of r_0 are considered for multiplicities 2, 3, and ≥ 4 and a linear depen-

TABLE II. Characteristic distances of the muon lateral distribution (Fréjus site); n is the true multiplicity. (a) Assuming no dependence on zenith angle. (b) Zenith-angle dependence in two bins of multiplicity. (c) Linear fit to zenith-angle dependence, $r_0(\cos\theta) = r_0(\gamma_n) + \alpha_n(\cos\theta - \gamma_n)$.

(a)

n	r_0 (cm)
2	174±3
3	162±7
≥4	142±3

(b)

$\cos(\theta)$	r_0 ($n \le 3$) (cm)	r_0 ($n \ge 4$) (cm)
0.500–0.638	194±7	158±7
0.638–0.716	179±6	153±7
0.716–0.772	182±6	141±7
0.772–0.821	166±5	151±7
0.821–0.867	175±5	143±6
0.867–0.905	163±5	142±6
0.905–0.946	167±5	123±6
0.946–1.000	161±5	127±6

(c)

	$n \le 3$	$n \ge 4$
γ_n	0.828	0.832
$r_0(\gamma_n)$ (cm)	171.0±1.8	138.8±2.4
α_n (cm)	−72.4±16.5	−85.0±20.7

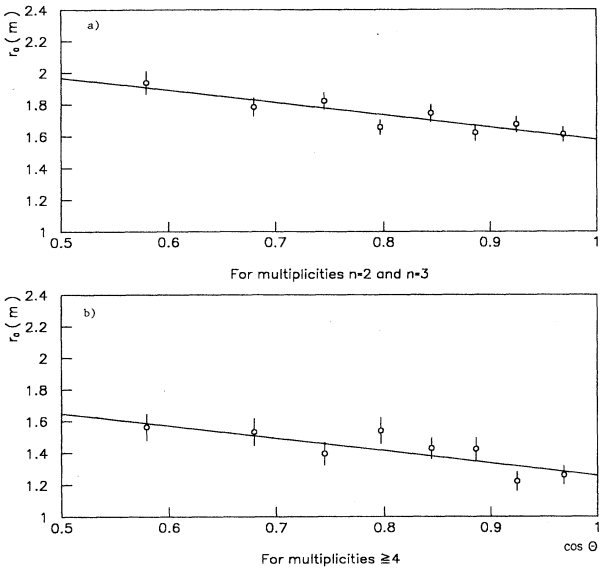

FIG. 6. Characteristic distances r_0 as a function of $\cos\theta$ (θ= zenith angle) (a) for events with multiplicity $n \leq 3$, (b) for events with multiplicity $n \geq 4$.

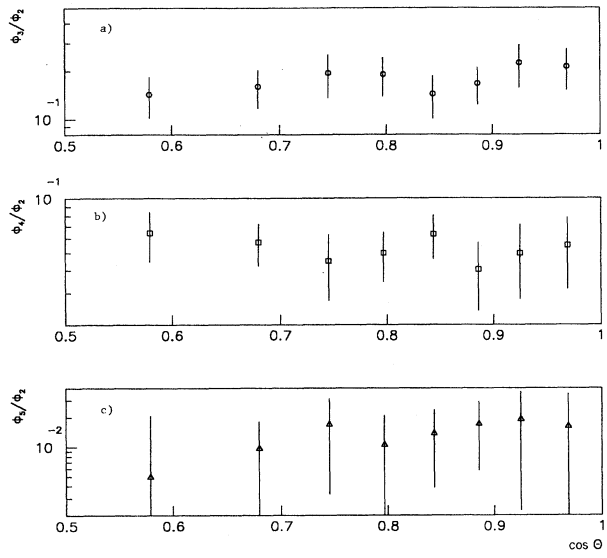

FIG. 7. Flux ratios (Φ_n/Φ_2) for different multiplicities n as a function of $\cos\theta$ (θ=zenith angle): (a) $n=3$, (b) $n=4$, (c) $n=5$.

dence on $\cos\theta$ is assumed with a slope independent of the multiplicity.

C. Results on the multiplicity distribution and fluxes

The shapes of the corrected multiplicity distributions obtained in the eight intervals in zenith angle are found to be compatible with each other (Fig. 7). Consequently, results are presented for the full range $\theta < 60°$. They are given in Table III for multiplicities smaller than or equal to six. For higher multiplicities, the fit yields large correlated errors so that it is more convenient to display the fluxes of events with a multiplicity $k \geq n$ ($F_n = \sum_{k \geq n} \Phi_k$) as a function of n (Fig. 8). For multiplicities $n \geq 2$, results are well fitted by the empirical formula

$$\Phi_n = \frac{K}{n^{\nu}} \quad (n \geq 2) \text{ with } \nu = \frac{\nu_1}{1+an} \tag{7}$$

with $K = (5.6 \pm 0.5) \times 10^{-5}$ m^{-2}s^{-1}, $\nu_1 = 4.63 \pm 0.11$, and $a = (0.66 \pm 0.16) \times 10^{-2}$, with a correlation coefficient for ν_1 and a of 0.918.

It is interesting to compare K with the flux for $n=1$. The latter is directly derived from the sample of single-muon events which is corrected for the small contamination (6%) of higher-multiplicity events calculated from the fluxes given above and from the preceding lateral distribution. This sample (407 775 events) was selected with the same criteria as multimuon events, but single muons were reconstructed by an automatic procedure with an efficiency of 92%. Taking this into account, one finds

TABLE III. Corrected fluxes averaged over shower directions with zenith angle $\theta < 60°$ (Fréjus site). Φ_n are the fluxes corresponding to a shower with n muons. F_n are the integral fluxes defined as $F_n = \sum_{k \geq n} \Phi_k$.

n	Φ_n (m^{-2}s^{-1})	F_n (m^{-2}s^{-1})
2	$(2.31 \pm 0.07) \times 10^{-6}$	$(2.91 \pm 0.05) \times 10^{-6}$
3	$(4.13 \pm 0.30) \times 10^{-7}$	$(6.08 \pm 0.29) \times 10^{-7}$
4	$(1.23 \pm 0.13) \times 10^{-7}$	$(1.95 \pm 0.10) \times 10^{-7}$
5	$(3.26 \pm 0.10) \times 10^{-8}$	$(7.26 \pm 0.68) \times 10^{-8}$
6	$(1.4 \pm 1.0) \times 10^{-8}$	$(3.99 \pm 0.60) \times 10^{-8}$
7		$(2.65 \pm 0.57) \times 10^{-8}$
8		$(1.56 \pm 0.50) \times 10^{-8}$
9		$(1.1 \pm 0.5) \times 10^{-8}$
10		$(9.3 \pm 5.0) \times 10^{-9}$

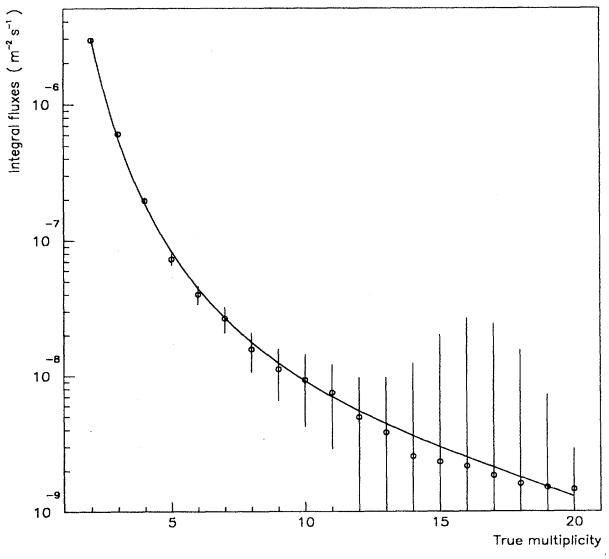

FIG. 8. Integral fluxes $F_n = \sum_{k \geq n} \Phi_k$ as a function of multiplicity n. The curve represents the distribution expected from formula (7) using the fitted values of ν_1 and a quoted in the text.

TABLE IV. Rock thickness (m) as a function of zenith and azimuth angles (Fréjus site).

Azimuth	Zenith angle (degrees)												
(degrees)	0	5	10	15	20	25	30	35	40	45	50	55	60
0	1635	1651	1687	1746	1821	1915	1915	1923	2013	2165	2484	3152	3481
5	1635	1646	1682	1726	1788	1888	2046	2032	2125	2298	2654	2988	3267
10	1635	1646	1671	1710	1756	1845	2032	2203	2354	2461	2754	2838	3025
15	1635	1644	1656	1693	1728	1809	1955	2145	2349	2584	2665	2780	2902
20	1635	1636	1648	1675	1704	1774	1891	2066	2257	2522	2639	2724	2829
25	1635	1635	1636	1653	1681	1740	1824	2004	2148	2417	2591	2683	2738
30	1635	1628	1624	1626	1653	1698	1801	1961	2073	2312	2521	2596	2724
35	1635	1615	1614	1612	1624	1674	1774	1911	2023	2180	2535	2660	2792
40	1635	1620	1602	1586	1593	1642	1715	1886	1970	2083	2380	2794	2943
45	1635	1610	1583	1568	1578	1619	1692	1870	1920	2031	2310	2937	3351
50	1635	1611	1576	1562	1552	1591	1647	1814	1879	1978	2241	2991	3418
55	1635	1603	1565	1548	1533	1562	1631	1769	1839	1923	2136	2817	3170
60	1635	1612	1555	1538	1542	1542	1612	1731	1824	1899	2074	2615	3025
65	1635	1605	1559	1521	1534	1514	1621	1705	1784	1872	2043	2467	2877
70	1635	1604	1554	1500	1519	1497	1601	1630	1740	1846	2020	2433	2657
75	1635	1595	1541	1485	1495	1486	1545	1626	1687	1819	1965	2308	2529
80	1635	1595	1550	1489	1468	1480	1507	1595	1664	1778	1918	2204	2337
85	1635	1593	1549	1485	1451	1452	1493	1591	1658	1776	1895	2045	2212
90	1635	1587	1554	1489	1454	1453	1486	1545	1674	1779	1898	2030	2079
95	1635	1571	1542	1488	1457	1451	1477	1534	1650	1742	1854	1968	2029
100	1635	1576	1543	1489	1463	1449	1470	1531	1612	1707	1895	1961	2009
105	1635	1569	1536	1498	1472	1466	1493	1552	1640	1768	1942	2024	2072
110	1635	1571	1540	1521	1477	1481	1521	1608	1705	1819	2084	2182	2201
115	1635	1567	1521	1522	1510	1523	1604	1670	1793	2057	2115	2185	2399
120	1635	1564	1510	1511	1499	1534	1601	1714	1909	2031	2167	2264	2397
125	1635	1563	1524	1510	1505	1533	1613	1825	1842	1918	2086	2238	2385
130	1635	1568	1525	1508	1512	1552	1660	1802	1799	1846	1955	2119	2361
135	1635	1565	1515	1504	1518	1568	1725	1788	1793	1829	1927	2012	2199
140	1635	1567	1533	1519	1523	1589	1778	1772	1781	1814	1885	1951	2106
145	1635	1571	1537	1527	1543	1623	1768	1753	1771	1817	1886	1954	2117
150	1635	1570	1543	1537	1552	1757	1745	1747	1786	1838	1953	2012	2148
155	1635	1574	1552	1545	1577	1736	1737	1759	1804	1883	2039	2107	2262
160	1635	1581	1564	1558	1604	1722	1725	1781	1876	1957	2068	2193	2373
165	1635	1587	1565	1573	1637	1701	1706	1726	1825	2039	2158	2324	2472
170	1635	1586	1570	1592	1669	1708	1695	1724	1814	2034	2168	2324	2500
175	1635	1587	1574	1601	1683	1715	1713	1734	1791	1905	2191	2293	2429
180	1635	1588	1584	1620	1712	1734	1727	1756	1785	1902	2046	2194	2365
185	1635	1594	1594	1636	1731	1758	1762	1771	1801	1886	2059	2163	2301
190	1635	1605	1604	1646	1785	1767	1768	1787	1814	1874	2046	2130	2328
195	1635	1607	1614	1665	1745	1768	1769	1777	1795	1876	2037	2118	2295
200	1635	1612	1627	1682	1703	1761	1765	1763	1795	1876	1990	2118	2359
205	1635	1625	1655	1688	1662	1731	1770	1788	1818	1887	1997	2106	2890
210	1635	1636	1665	1665	1648	1685	1781	1809	1859	1948	1997	2116	3380
215	1635	1646	1686	1655	1629	1635	1731	1858	1907	1956	2025	2125	2990
220	1635	1646	1679	1646	1638	1610	1660	1753	1905	1955	2027	2160	2747
225	1635	1659	1667	1620	1598	1589	1605	1698	1803	1941	2021	2197	3118
230	1635	1666	1652	1599	1576	1562	1564	1631	1709	1773	1978	2261	3468
235	1635	1686	1645	1585	1560	1546	1555	1592	1676	1731	1829	2139	2794
240	1635	1693	1647	1581	1542	1524	1527	1557	1632	1685	1766	1925	2255
245	1635	1693	1638	1581	1551	1519	1533	1546	1588	1633	1710	1836	2070
250	1635	1704	1653	1599	1551	1513	1544	1559	1611	1641	1703	1770	1970
255	1635	1696	1652	1605	1553	1518	1545	1556	1601	1655	1704	1774	1923
260	1635	1710	1656	1623	1549	1522	1547	1571	1600	1665	1721	1780	1933
265	1635	1719	1690	1617	1563	1572	1570	1575	1632	1677	1818	1887	1965
270	1635	1727	1685	1626	1552	1535	1566	1611	1662	1707	1793	1892	2004
275	1635	1727	1685	1628	1564	1558	1585	1612	1639	1703	1780	1871	1962
280	1635	1746	1698	1626	1576	1589	1614	1608	1645	1703	1758	1784	1858
285	1635	1746	1700	1633	1590	1619	1607	1621	1662	1716	1743	1779	1859
290	1635	1744	1707	1632	1617	1654	1630	1644	1673	1719	1739	1805	1890

TABLE IV. (*Continued*).

Azimuth (degrees)	Zenith angle (degrees) 0	5	10	15	20	25	30	35	40	45	50	55	60
295	1635	1746	1706	1650	1633	1678	1647	1669	1697	1718	1752	1815	1914
300	1635	1727	1720	1670	1661	1700	1669	1684	1677	1704	1755	1820	1923
305	1635	1722	1732	1694	1689	1726	1697	1675	1659	1684	1730	1788	1873
310	1635	1709	1748	1717	1732	1711	1675	1658	1660	1681	1727	1828	1972
315	1635	1702	1766	1757	1730	1674	1665	1645	1626	1665	1763	1920	2027
320	1635	1700	1766	1754	1690	1658	1675	1664	1646	1699	1783	1954	2050
325	1635	1678	1741	1749	1690	1678	1715	1696	1679	1724	1851	1969	2101
330	1635	1677	1728	1755	1702	1703	1735	1706	1691	1737	1895	2014	2209
335	1635	1672	1726	1777	1725	1730	1769	1753	1736	1767	1912	2087	2345
340	1635	1667	1716	1779	1745	1774	1796	1770	1765	1857	1982	2197	2524
345	1635	1667	1707	1804	1783	1815	1800	1802	1801	1892	2063	2320	2719
350	1635	1662	1700	1790	1834	1826	1810	1806	1864	2010	2209	2509	3421
355	1635	1658	1698	1761	1873	1865	1840	1858	1932	2059	2288	2833	3776

$\Phi_1=(5.47\pm0.10)\times10^{-5}$ $m^{-2}s^{-1}$, showing that formula (7) can be extrapolated to $n=1$. It should be noted that the error on Φ_1 is dominated by systematics on the muon reconstruction efficiency.

D. Consistency checks

In order to check the rather complex method used above, a simple Monte Carlo program simulating the experimental effects (detector size, trigger conditions, and selection criteria) was written. Events were generated using the observed angular distribution, the multiplicity distribution given by (7) and the lateral distribution characterized by Table II(b). An excellent agreement was observed with raw data, namely, with the distributions of observed distances (Fig. 4) and raw multiplicities (Fig. 3).

V. CONCLUSIONS

The variation of the vertical muon intensity with depth in the 4000–9000-hg/cm^2 range was found to be in agreement with previous experimental results.[6]

Because of the large dimensions of the Fréjus detector with respect to the shower size, both the lateral distribution and the multiplicity distribution of muon bundles were determined experimentally. To our knowledge, this is the first time that such results are presented corrected for experimental biases, particularly, for the limited size of the detector.

(a) Lateral distribution. The characteristic distance r_0 [defined by formula (1)] is found to decrease linearly with the cosine of the zenith angle θ for $\theta<60°$. The distance r_0 is found to decrease significantly when the muon multiplicity increases from $n=2$ to $n=4$. One finds

$$\Delta r_0=r_0(n\leq3)-r_0(n\geq4)=32\pm3 \text{ cm} .$$

It should be noted that, since about 60% of the events in the $n\geq4$ sample are genuine four-muon showers, a different behavior of r_0 for larger multiplicities is not excluded.

(b) Muon multiplicity distribution. The multiplicity distribution is well described by formula (7), which significantly deviates from a power law. This fit is well constrained by the data for $n\lesssim10$.

The preceding results should be compared with predictions of air-shower simulations in the framework of various primary composition models. Such calculations involve many parameters and are further submitted to uncertainties in hadronic physics in the 10^2–10^4-TeV primary energy range. It should be noted, however, that only a few parameters actually influence the prediction of the shape of the multiplicity distribution, i.e., of the quantities ν_1 and a of formula (7). Therefore, the high statistics and large detection area of the Fréjus experiment should enable us to provide more constraints on cosmic-ray composition models. This will be done in a forthcoming publication.

ACKNOWLEDGMENTS

The work at Aachen was supported by the Bundesminister für Forschung und Technologie (BMFT), Federal Republic of Germany (FRG), under Contract No. 55 AC 14 P. Laboratoire de l'Accélérateur Linéaire and Laboratoire de Physique Nucléaire des Hautes Energies are Institut National de Physique Nucléaire et de Physique des Particules du Centre National de la Recherche Scientifique. Département de Physique des Particules Elémentaires is Institut de Recherche Fondamentale du Commissariat à l'Energie Atomique. The work at Wuppertal was supported by the BMFT, FRG, under Contract No. 55 WT 84 P.

APPENDIX: CHARACTERISTICS OF THE FRÉJUS SITE

Table IV yields the rock thickness (in meters) for a direction defined by the zenith angle θ and the azimuth. The origin of azimuths is given by the longitudinal axis of the detector (making a 15.1° angle with the East-West direction) oriented from East to West. These tables were obtained by digitizing the topographic maps of the French National Geographical Institute (IGN) (scale 1/25 000), the detector coordinates being 6°41′21″ E and 45°8′32″ N.

Rock thickness can be converted into hg/cm^2 of standard rock by the classic procedure explained in Ref. 10, on the basis of the Fréjus rock density (2.73 ± 0.01 g cm^{-3}) and of its chemical composition, the latter being essentially characterized by the quantity $\langle Z^2/A \rangle = 5.87 \pm 0.02$, the average being taken over all constituents with weights equal to their mass fraction. The $\langle Z/A \rangle$ ratio is practically identical to that of standard rock (0.50).

---

*Permanent address: Lawrence Berkeley Laboratory, Berkeley, CA 94720.

†Present address: Istituto di Fisica, Universita di Milano, Milano, Italy.

‡Present address: Dornier GmbH, Friedrichshafen, Federal Republic of Germany.

§Present address: Fisher Controls GmbH, Solingen, Federal Republic of Germany.

[1]T. K. Gaisser and T. Stanev, Nucl. Instrum. Methods **A235**, 183 (1985).

[2]B. Degrange and S. Tisserant, Invited talk at the Xth European Cosmic Ray Symposium, Bordeaux, France, 1986, edited by M. F. Bourdeau, J. N. Capdevielle, and P. Gabinski (unpublished), p. 208.

[3]A. A. Watson, in *Proceedings of the XIXth International Cosmic Ray Conference,* La Jolla, California, 1985, edited by P. C. Jones, J. Adams, and G. M. Mason (NASA Conf. Publ. 2376) (Goddard Space Flight Center, Greenbult, MD, 1985), Vol. 9. p. 111; T. Stanev, *ibid.*, p. 383.

[4]F. Ellenberger, *Etude Géologique du pays de la Vanoise,* edited by Bureau de Recherches Géologiques et Minières, Paris, 1958 (Mém. Carte Géol. Fr., Paris, 1958).

[5]Ch. Berger *et al.*, Nucl. Instrum. Methods **A262**, 463 (1987).

[6]For a world survey of muon vertical intensity versus depth, see M. Crouch, in *Proceedings of the XXth International Cosmic Ray Conference,* 1987, edited by V. A. Kozyarivsky *et al.* (Nauka, Moscow, 1987), Vol. 6, p. 165; see also, G. Battistoni *et al.*, *Proceedings of the XIXth International Cosmic Ray Conference* (Ref. 3), Vol. 2, p. 158.

[7]J. W. Elbert, T. K. Gaisser, and T. Stanev, Phys. Rev. D **27**, 1448 (1983).

[8]The average distance between a muon and the shower axis is thus $2r_0$ and the average distance between two muons is $(15\pi/16)r_0$.

[9]L. Behr, Ph.D. thesis, Paris, 1965; S. Tisserant, Ph.D. thesis, Paris, 1987.

[10]A. G. Wright, *Proceedings of the XIIIth International Cosmic Ray Conference,* Denver, 1973 (Colorado Associated University Press, Boulder, 1973).